Time expansion chamber system for characterization of TWIST low-energy muon beams

J. Hu[a], G. Sheffer[a], Yu.I. Davydov[a,b], D.R. Gill[a], P. Gumplinger[a], R.S. Henderson[a], B. Jamieson[a], C. Lindsay[a], G.M. Marshall[a,*], K. Olchanski[a], A. Olin[a], R. Openshaw[a], V. Selivanov[b]

[a]TRIUMF, 4004 Wesbrook Mall, Vancouver, BC, Canada V6T 2A3
[b]RRC "Kurchatov Institute", Moscow 123182, Russia

Abstract

A low-mass time expansion chamber (TEC) has been developed to measure distributions of position and angle of the TRIUMF low-energy surface muon beam used for the TRIUMF Weak Interaction Symmetry Test (TWIST) experiment. The experiment is a high-precision measurement of muon decay and is dominated by systematic uncertainties, including the stability, reproducibility, and characterization of the beam. The distributions measured by two TEC modules are one essential ingredient of an accurate simulation of TWIST. The uncertainties, which are extracted through comparisons of data and simulation, must be known to assess potential systematic uncertainties of the TWIST results. The design criteria, construction, alignment, calibration, and operation of the TEC system are discussed, including experiences from initial beam studies. A brief description of the use of TEC data in the TWIST simulation is also included.
© 2006 Elsevier B.V. All rights reserved.

1. Introduction

The TRIUMF Weak Interaction Symmetry Test (TWIST) measures momentum and angle distributions of positrons from the decay of highly polarized positive muons, to determine precisely the decay [1–3] parameters. It uses a solenoidal spectrometer with 2 T magnetic field consisting of 56 planar drift and proportional chambers arranged symmetrically with high precision on either side of a central foil that stops the low-energy muon beam [4]. The incident polarized muon beam is directed along the axis of the solenoid from the beam line, through the fringe field region, and into the chamber stack within the uniform tracking region. Following the decay of the muon, the positron is tracked in the chambers and a high-statistics decay distribution is acquired. The first results from the

experiment have been published [5,6]. To extend those results to higher precision, and especially to analyze and assess systematic uncertainties for the polarization-dependent asymmetry decay parameter $P_\mu \xi$ [7], a method was required to measure quickly and reliably the muon beam characteristics near the entrance to the solenoid. While the TWIST detector itself, specifically the first several planes of drift chambers, has some excellent properties for this kind of measurement, its placement is disadvantageous. It is located after materials that contribute to multiple scattering, such as a vacuum window and trigger scintillator. In addition, the gas density at atmospheric pressure and the extra cathode layers of the first detector chambers add intolerable scattering sources.

1.1. Muon beam characteristics

The requirements of high polarization and rapidly achieved high statistics are satisfied by a beam of surface

---

muons [8] produced at the surface of the primary proton target from pion decay at rest. High polarization with respect to the direction of momentum $\vec{p}$ ($P_\mu^{\vec{p}}$, which is exactly -1 if the Standard Model holds true) is assured, because the helicity of the muon neutrino determines the spin angular momentum of the recoiling muon. The resulting muons have momentum of $29.79\,\text{MeV}/c$ ($4.12\,\text{MeV}$) and a range of only $0.15\,\text{g/cm}^2$ in carbon.

For the TRIUMF M13 beam line [9], the primary production target is typically graphite of thickness $10\,\text{mm}$. At the momentum of surface muons, there are also other particles in the beam, such as positrons, positive pions, protons, and heavier positive ions. However, the pion decay length is short compared to the channel length, while protons and heavier ions do not penetrate thin material layers, leaving positrons as the major beam contaminant. They can be readily distinguished from surface muons by a combination of energy loss and time of flight with respect to the 43 ns period of the accelerator. The time of flight also permits separation of a small component of muons which arise from pion decay in flight. While the maximum surface muon rate for the beam line is of order $10^6\,\text{s}^{-1}$, the TWIST experiment selects muons to provide a small beam spot, divergence (see Section 4), and momentum spread. The muon rate is typically $1-5 \times 10^3\,\text{s}^{-1}$.

Those muons that are created within the primary target, some distance from its surface, will lose energy and undergo multiple scattering prior to escaping into the surrounding vacuum. Some scattering can also occur in any materials in the beam line between the primary target and the TWIST detector. Scattering reduces the correlation of momentum and spin directions, and thus the polarization, so it is essential to eliminate such materials as much as possible and to select only those muons near the maximum momentum allowed in the decay to keep this depolarization at a level negligible compared to the sensitivity of the TWIST measurements.

These criteria demand a muon beam line with momentum resolution $\Delta p/p \sim 0.01$ (FWHM) [9], with no significant windows, residual gas, or other material in the muons' path. The muons transported to the end of the beam line by magnetic elements will retain the correlation of momentum and spin direction, $P_\mu^{\vec{p}}$. The ensemble polarization of the beam with respect to a beam axis $\hat{z}$, $P_\mu^{\hat{z}}$, will be less than $P_\mu^{\vec{p}}$ for a beam of finite emittance, but a high and predictable correlation of momentum and spin is retained.

As the muon traverses the beam line, the solenoid fringe field region, and enters the tracking region, the momentum and spin direction retain their correlation ($P_\mu^{\vec{p}}$ is preserved), but transverse momentum components are added in the fringe field and an apparent depolarization with respect to the solenoid (and beam) axis is the result, i.e., $P_\mu^{\hat{z}}$ decreases. This can be modeled quite precisely in simulations, assuming the field shape is known sufficiently well, and also assuming the particle positions and momenta can be determined for some point near the entrance to the field.

A detector to measure muon positions and momentum directions in a surface muon beam has been constructed, using two time expansion chambers (TECs) [10] at low pressure. A low pressure ($4-40\,\text{mbar}$) proportional chamber was tested in Ref. [11]. Detailed investigations of low-pressure chambers were described in Ref. [12]. A TEC determines the track of an ionizing particle in one dimension, transverse to the particle's direction, via the drift time of ionization in a relatively uniform drift field. The ionization then reaches a region of higher field where gas amplification takes place near a sense-wire anode. Because beam characteristics are required for both dimensions (x and y) transverse to the beam direction (z), the TWIST TEC system consists of two orthogonal TEC modules.

2. Design, construction, and operation

Surface muons are easily scattered, so to minimize multiple scattering effects, the primary design criterion for the TWIST TEC system was to maintain low mass. The detector must also operate in the vacuum of the muon beam channel, which in this case is not isolated from the primary production target nor from the accelerator itself. Operation of the detector using low-pressure dimethyl ether (DME) gas allows the use of thin windows that isolate the chamber gas from the beam line vacuum. DME, having a long drift time, small Lorentz angle, and high primary ionization, is convenient because it is also used for TWIST drift chambers. An automated control system ensures that this low differential pressure is maintained. The overall length of the TEC system was kept to a minimum compatible with a reasonable track length necessary for an accurate direction measurement. The beam size can range up to a few centimeters, so a somewhat larger active area was chosen, within which the only materials in the beam path are the entrance and exit windows, the low-pressure chamber gas, and very thin field cage wires required to define the drift field. The device must be capable of recording muon rates up to several thousand per second, while its operation should also not be compromised by a comparable rate of beam positrons.

Even though the TEC material in the beam path has been minimized, it scatters the beam too much to be used simultaneously during TWIST's highest precision muon decay polarization measurements. The total systematic uncertainty grows as the depolarization increases, so the TEC system is removed for most muon decay data taking. Instead, it is used periodically to tune and measure characteristics and to verify muon beam stability between beginning and end of data sets taking several days to collect. In this way, possible muon beam changes during the data set collection become evident, which may be correlated to other carefully monitored quantities. Therefore, another important design feature was that the

detector can be installed into and removed from the beam line quickly, conveniently, and reproducibly.

2.1. Design of the TEC system

The TEC system is located directly upstream of the TWIST spectrometer and is attached to the end of the TRIUMF M13 beam line [9] as shown in Fig. 1. The beam passes from the final two quadrupoles through a gate valve and into the low-pressure gas containment volume in which the two TEC modules operate. It then continues in vacuum through the fringe field near the yoke end plate until it reaches a vacuum window inside the high-field region. From there, it passes through a variable density gas degrader, a thin trigger scintillator, and into the TWIST detector.

As can be seen in Fig. 2, the TEC system consists of two identical modules rotated 90° with respect to each other and mounted in an aluminum gas box of length 280 mm. One module tracks the horizontal (x) position and angle of the incoming muons and the other the corresponding vertical (y) components. Each module is 80 mm long. The active area that can be measured by each TEC is 60 mm × 60 mm transverse to the beam, with an active length of 48 mm (24 wires spaced by 2 mm). The gas box has 6 μm aluminized Mylar entrance and exit windows and is nested in a vacuum box. The pressure is maintained at 80 mbar with a flow of DME gas of approximately 100 cm³/min. The vacuum box is part of the beam line

and remains in place, while the TECs, the gas box, and the gas box lid can be removed and replaced by a blank cover plate.

Fig. 3 shows an exploded three-dimensional rendering of one TEC module. The sense and grid planes are strung on frames of nominally 1.6 mm thick G-10 (epoxy/glass) printed circuit boards (PCBs) as are the side walls of the field defining cage. The drift field plane frames are 3.2 mm thick PCBs. The remaining structural elements of the module are also manufactured from G-10. The connectors have gold plated contacts in a glass-filled polyester matrix. The module is assembled with nylon cap screws. All materials have been tested for compatibility with the DME gas [13].

Each module contains a drift field region and gas amplification region. The drift field region is bounded by a four-sided field defining cage with two side wall elements containing parallel horizontal printed circuit traces and two end (particle entrance and exit) field planes with 50 μm gold plated Cu/Be wires strung horizontally across the opening. The wires of the two end drift field planes are electrically connected to the side wall traces through gold plated pins and a socket assembly. The pitch of the wires and traces is 2.54 mm. To achieve a uniform electric field, each group of wires and traces is connected to its neighbor through resistors of the same value creating a resistor chain to which high voltage is applied. The drift cathode plane on the bottom of the field cage is a copper foil on a 1.6 mm G-10 substrate.
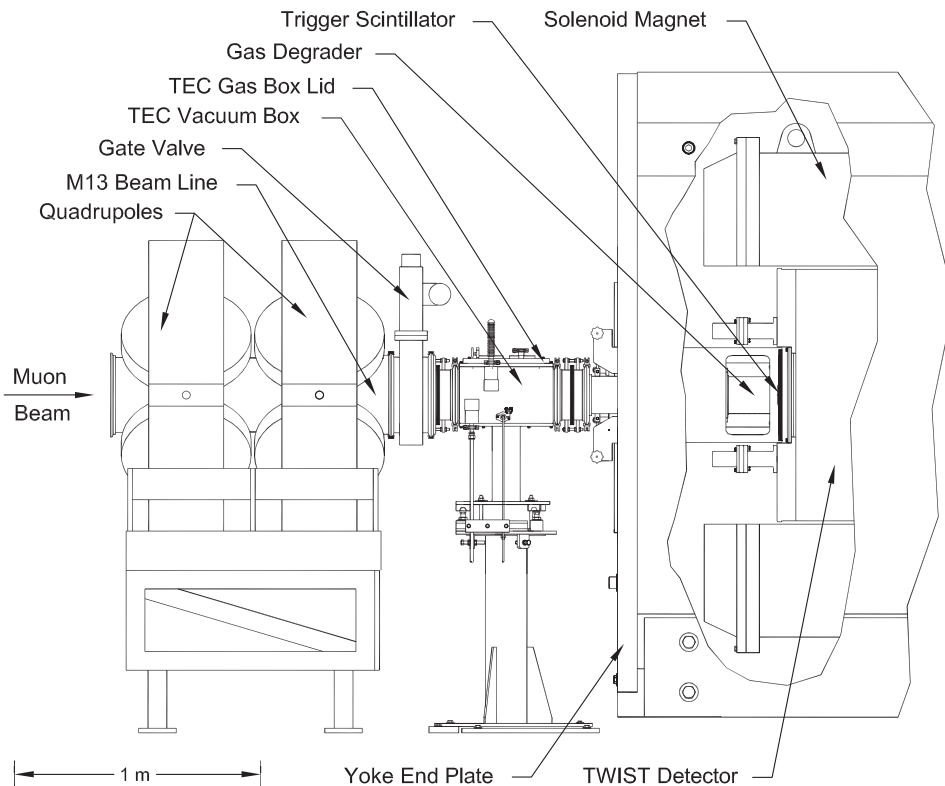

Fig. 1. Placement of the TEC system in the muon beam between the exit of the beam line and the TWIST solenoid.
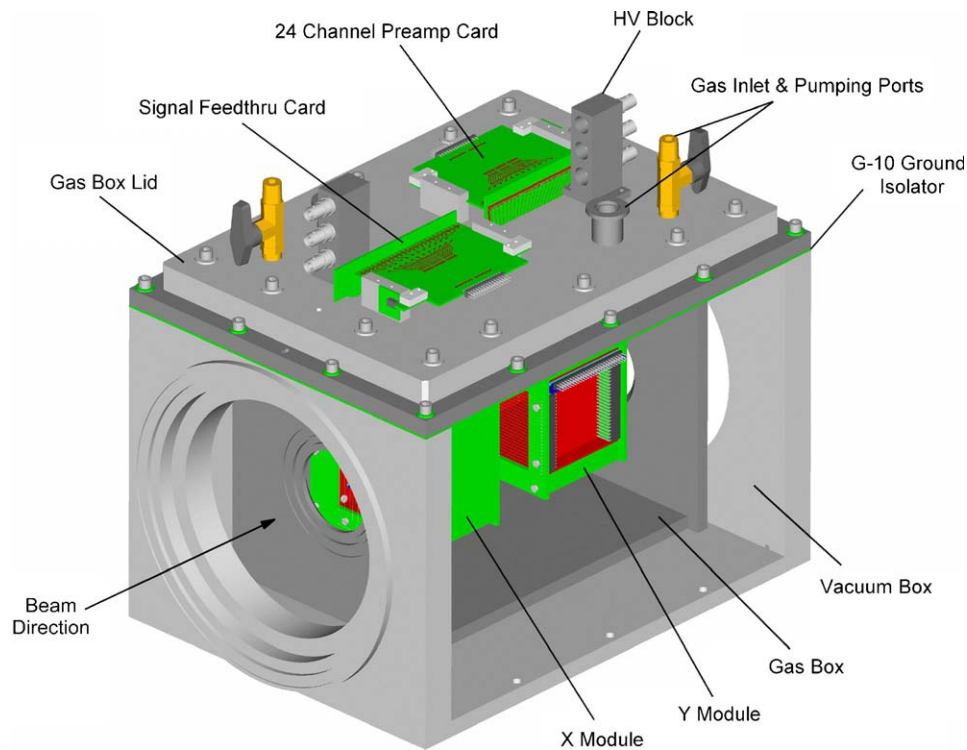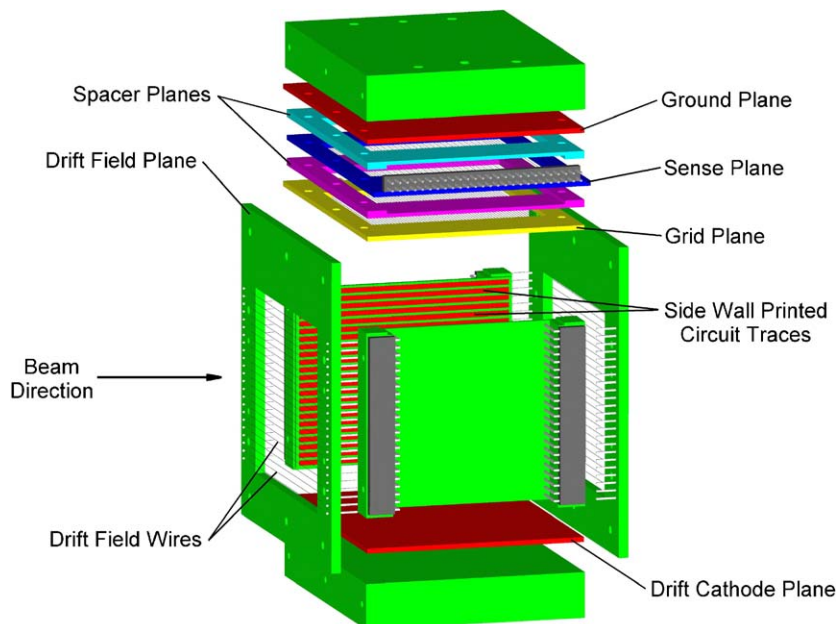
Fig. 2. TEC modules in the gas box.

Fig. 3. Exploded three-dimensional view of one TEC module.

The gas amplification region consists of a grid wire plane, a sense-wire plane and a solid cathode plane. These planes are separated by spacer planes made of 1.6 mm G-10. A section of the wire geometry of this configuration is shown in Fig. 4. The grid and shield wires are 125 μm gold plated Cu/Be. The sense wires are 25 μm gold plated tungsten. The signals from the 24 sense wires are taken from the end of the PCB through a coaxial cable assembly to a feedthrough in the gas box lid.

When the elements of the drift field region and gas amplification region are mated, the last resistor in the field defining cage is connected to the grid plane, which is maintained at ground potential as is the ground plane on the other side of the sense plane. As shown in Fig. 4, the
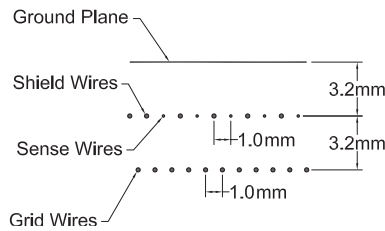
Fig. 4. Sense plane geometry.

sense plane is made up of alternating sense and shield wires. Gas amplification occurs only at the thinner sense wires. The diameter of $25\,\mu m$ was chosen for these wires based on our previous study of gas gain at low pressure [14]. The shield wires screen the induced pulses from adjacent wires and are necessary because the average angle of the muon tracks through the TEC module is quite small. This results in signals on adjacent sense wires occurring at very nearly the same time, so the mutually induced pulses would seriously affect the rise time of these signals and hence the accuracy of the drift time measurement.

2.2. TEC alignment

It is important to align the TEC system accurately with respect to the TWIST spectrometer and hence with the measured magnetic field map. Cross-hairs were mounted in the apertures at each end of the steel yoke of the spectrometer to define the z-axis. An optical surveying instrument (theodolite) was then used to align each TEC to these cross-hairs. First the x and y positions of the TEC system were adjusted to align the field cage wires for both x and y modules, and then the location was checked with the position of the central hole of the calibration collimators (see Section 3.2). The accuracy was approximately $\pm 250\,\mu m$. Once this alignment was completed another optical device, a Leica TDA5005 Total Station, was used to record the position of the TEC vacuum box with respect to the M13 beam line and TWIST spectrometer.

As described previously, the TECs, the TEC gas box, and the gas box lid have been designed to be easily removed and replaced. This is done in a reproducible manner using locating pins in the vacuum box, which remains as part of the beam line vacuum system with a blank cover plate. However, any time the TEC assembly is removed and replaced, a measurement of its position is made with the Total Station to confirm that proper alignment has been maintained. The accuracy of this measurement is $\pm 50\,\mu m$. It was necessary to take precautions to avoid movement due to forces from vacuum loading of the beam line and magnetic fields of the solenoid.

2.3. TEC operation

The optimum drift field for the TECs was found to be approximately $16\,V/mm$, corresponding to an applied drift cathode plane voltage of $-1000\,V$ with the grid plane at

ground potential (refer to Fig. 3). The applied sense-wire high voltage is $1150\,V$ and the shield wires are at $300\,V$. These voltages result in a muon track efficiency of essentially 100% with typically up to 19 out of 24 wires providing measurable ionization signals (hits) per muon track (see Section 3.3). There are intermittent sparks, the location and cause of which are still undetermined. A degradation of efficiency over a period of weeks of operation has also been observed, which may be a result of the sparking. Although the origins of these effects are not yet understood, the practical solution of regular replacement of sense-wire planes has been adopted.

2.4. Electronics and readout

The 24 wires of each of the TEC modules are connected to 24-channel preamplifiers mounted on the lid of the TEC gas box. The preamplifiers were developed at Fermilab for use at their Colliding Detector Facility [15]. Each channel has a gain of $1\,mV/fC$ and a dynamic range of -400 to $+20\,fC$. Signals are taken via $9.5\,m$ of microcoaxial cable to custom made post amplifier/discriminator modules, which have 16 channels in a single width CAMAC module and are also used in the readout of the TWIST spectrometer [4]. The resulting discriminated ECL logic signals are then sent via $15\,m$ of twisted pair cable to separate channels of a 64-channel LeCroy 1877 FASTBUS time-to-digital converter (TDC). These TDCs are multi-hit type to allow digitization of up to eight time intervals per channel per readout (or event). They have $0.5\,ns$ resolution and are operated in common stop mode. The trigger signal for the TDCs is derived from a plastic scintillator mounted downstream of the TEC vacuum box. When the solenoid is in operation, it is the same scintillator that provides the trigger for TWIST (as shown in Fig. 1); a dedicated trigger scintillator following a window at the exit of the TEC vacuum box is used for tests and tuning with the solenoid magnetic field off.

2.5. Gas system

The TEC gas system is required to provide a flow (typically $100\,cm^3/min$) of DME to the TECs while maintaining a constant pressure (typically $80\,mbar$) in the gas box. Upstream pressure control is accomplished with an absolute pressure transducer that measures the pressure in the TEC volume. This transducer signal is fed to a proportional-integral–differential (PID) device controlling the flow through a mass flow controller in the gas supply line to the TECs. Downstream flow control is provided by a manual 15-turn metering needle valve in the exhaust line between the TECs and the exhaust pump. The observed pressure control stability, as reported by the pressure transducer, is approximately $\pm 0.1\%$. The manufacturer's specifications for the pressure transducer indicate an absolute accuracy (combined linearity, hysteresis, and non-repeatability) of $\pm 0.25\%$ and a temperature drift of

$-0.048\%/^{\circ}$C at the typical operating pressure. Issues pertaining to TEC gas box installation, gas control, and interlock features, are discussed in Appendix A.

3. Calibration and tracking

3.1. Field distortion

The field cage is used to produce a uniform drift field for electrons. Ideally, the electric field between the drift cathode plane and the grid plane (Fig. 3) is perpendicular to the planes and constant at $E = -1000/60.96 \approx -16.4$ V/mm everywhere in the drift volume. In reality, however, the field distribution is distorted by the high voltage applied to the sense plane and also by the stray electric field from the other TEC module.

The FEMLAB Program [16] was employed to study such effects. Fig. 5, obtained from the FEMLAB simulation of a single module, shows distributions of the drift fields in the center of the drift volume (i.e., at $x = 0$ for the X module) at various settings. Compared with the case when the sense plane is off (open circles), the field changes by about 10% over the length of the module when the sense plane is turned on (open squares), which indicates that the grid plane is not completely effective in shielding the drift region from the sense plane potential. A z position dependency of the field intensity is clearly seen in both cases. This edge effect is likely due to the influence of the field cage. In a test with FEMLAB, the grid plane was extended to cover the gap between the edge of the grid plane and the field cage, and the field cage wires were replaced with aluminized Mylar strips. The edge effects are then reduced significantly. With the sense plane off, the drift field is nearly constant across the module (filled triangles). Because the aluminized Mylar strips introduce more multiple scattering
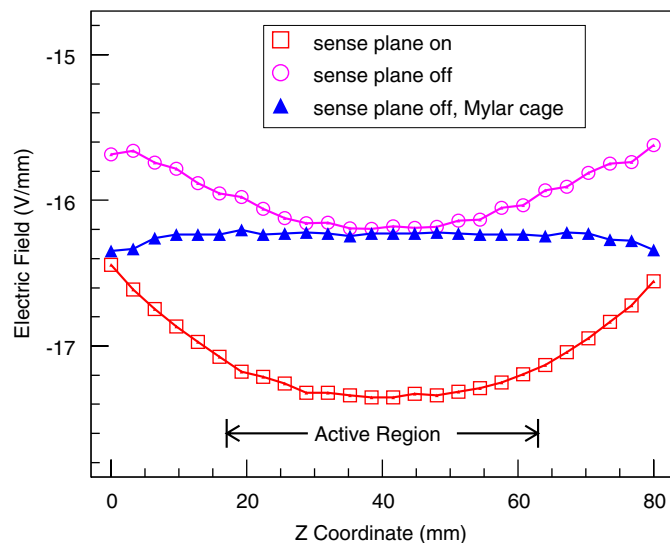
into the beam, they were not used in the actual TEC modules. Instead, field variations were accounted for via the position-dependent calibration procedure described in the next section.

Another source of field distortion comes from interference between the two modules. Fig. 6 is a contour plot of the change of field in the drift region of the X module when the Y module is turned on. This could bias the beam angle measurements by up to roughly 5 mrad even though the interference effect is on the order of 1%.

3.2. Extraction of space–time relationship

Precise characterization of the muon beam requires an adequate space–time relationship (STR, providing the relation between the distance of a muon track to the sense wires and the transit time to those wires of electrons produced by ionization along the track) for a TEC cell, which is defined by two neighboring shield and grid wires with a sense wire in the middle. As described in the previous section, the electric field in the drift region is not uniform. The drift velocity varies with the drift distance and the z position of the sense wire. A pair of multi-hole apertures, installed 141 mm upstream and downstream with respect to the center of the TEC gas box, acts as a collimator and is used as an external reference system to measure the STR as a function of various operating parameters. Each aperture, as shown in Fig. 7, consists of a square array of 7×7 holes, 1.2 mm in diameter, separated by 5.00 mm. The hole positions were measured to an accuracy better than 40 μm. Calibration data were obtained with a diffuse beam tune so that all holes have exposure

Fig. 5. Calculated drift field at the center ($x = y = 0$) of a single module. Sense-wire plane on and off are shown to demonstrate the effect on the dominant field. The active region, where the sense wires are located, is from $z = 17$ to 63 mm.
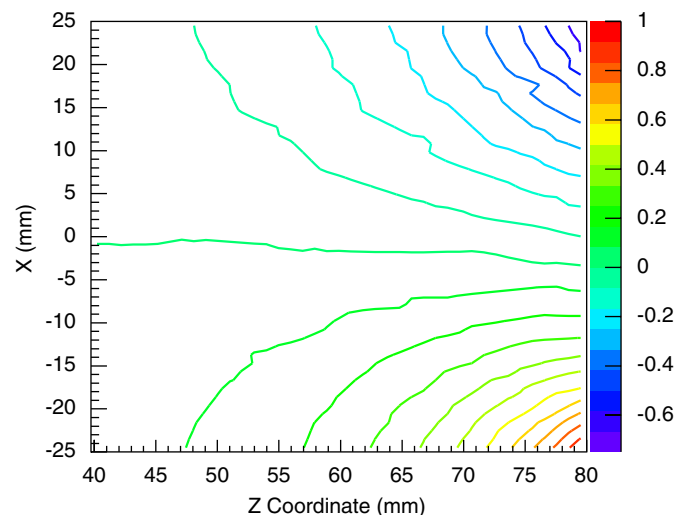

Fig. 6. Contours of calculated electric field contribution in the X module at $y = 0$, due to field leakage from the Y module. Color-coded contours show the field change in percentage (right-hand color scale) of the nominal central field (16.4 V/mm) of the X module. The difference in the x component of the field, when the Y module is turned on, is plotted in the portion of the drift region of the X module nearest the Y module. The z coordinates on this scale for the field cage of the Y module are $z = 120-200$ mm.
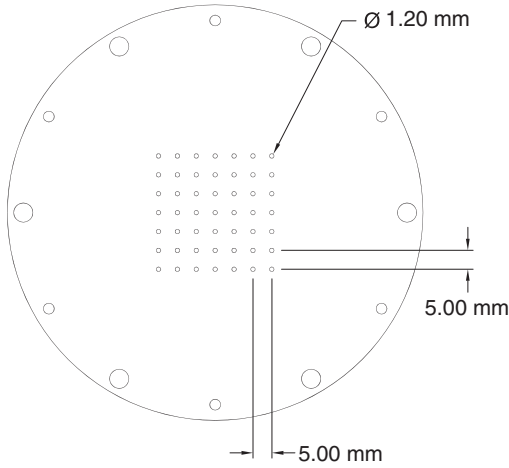
Fig. 7. A schematic plot of an aperture array. One is placed at each end of the TEC gas box to define tracks to be used for calibration.
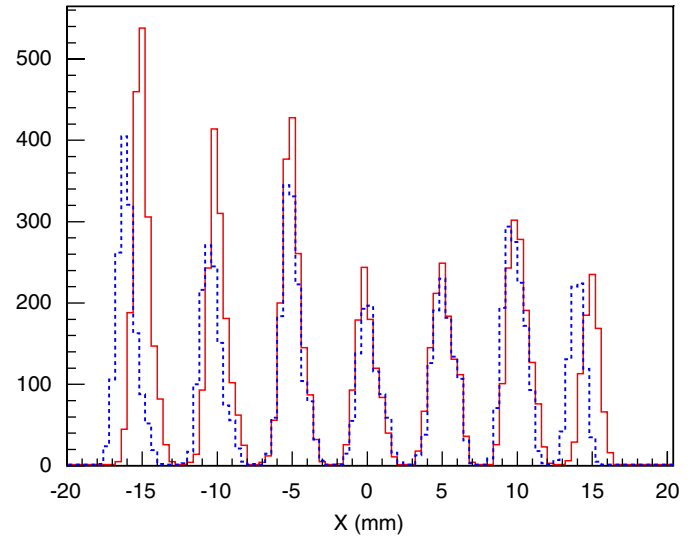

Fig. 8. Projection in x of measurements for muons passing through holes in one row of the collimator prior to calibration (blue dotted line, based on GARFIELD without field leakage) and following calibration (solid red line).
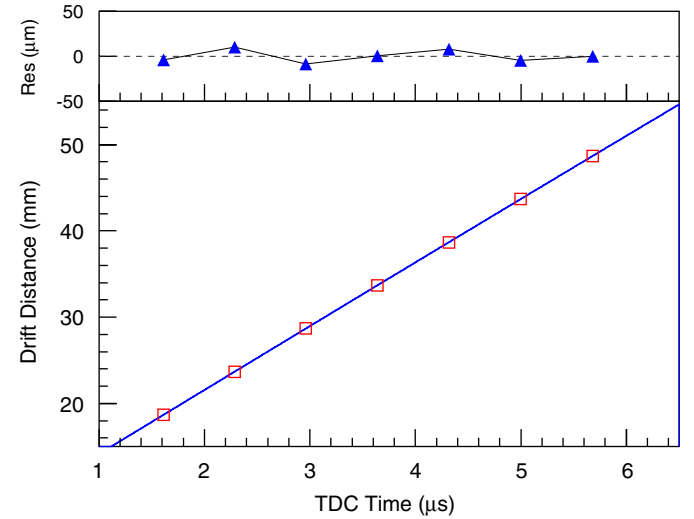

Fig. 9. Fit of the drift distance to the uncorrected TDC time to derive the STR. The plot at the top of the figure gives the residual of the fit.

from the beam. Beam tracks were selected with an angle near 0 mrad for calibration purposes, and it was verified that these tracks passed through corresponding holes in each of the two multi-hole apertures of the collimator. An example of a projection of measured x positions from one row of the aperture array is shown in Fig. 8, before and after the calibration procedure.

A third order polynomial function was used to fit the STR:

$$d_{ij}^k = p_0^k + p_1^k * t_{ij}^k + p_2^k * (t_{ij}^k)^2 + p_3^k * (t_{ij}^k)^3$$
$$(k = 1, \ldots, 48 \text{ and } i,j = 1, \ldots, 7),$$

where d_{ij}^k is the distance in x or y between the kth sense wire and a straight track connecting corresponding holes in the ith row and the jth column of the two multi-hole apertures; t_{ij}^k is the corresponding mean drift time. Fig. 9 presents an example of the fit quality. The cubic term reduces residuals by 10–20%; higher order terms were found to be negligible. With d in cm and t in μs, the linear term is of order one, while the quadratic and cubic terms are of order 10^{-2} and 10^{-3}, respectively. The drift times for ionization electrons in the active volume of the TEC are up to 8 μs.

While the calibration procedure has been shown to be quite adequate for the central active area of the TECs (30 × 30 mm^2) corresponding to the collimator described above, it is likely that the derived STR is not as accurate at the extremities. Apertures that cover the entire active region will be used in the future.

Simulations with GARFIELD [17] suggest that the drift time has an almost linear relationship with temperature and therefore gas density (as illustrated at a field of 16.4 V/mm in Fig. 10). Data taken at 19.6 and 23.0 °C confirm the temperature dependence. Because the DME gas pressure is fixed at 80 mbar and the temperature is recorded by the data acquisition system, variations of the STR with the gas density have been taken into account either by taking the calibration data at the same temperature or by linearly rescaling the STR according to the density.

3.3. Tracking resolution

In this paper, we use the word "event" to refer to the information which is recorded for each occurrence of a valid trigger. The trigger for readout of an event in the TEC system is provided by a signal from a single plastic scintillator placed after it. Associated with the trigger within a time window of −6 to +10 μs, one, or rarely more than one, muon may pass through the TECs. Ionization detected above the electronics threshold by a sense wire within the 16 μs time interval will be referred to as a "hit". Minimum ionizing positrons are also present in the beam, but are detected only with very low efficiency in the low-density gas. In fact, even muons above 50 MeV/c are not tracked efficiently with 80 mbar pressure. Regardless of the
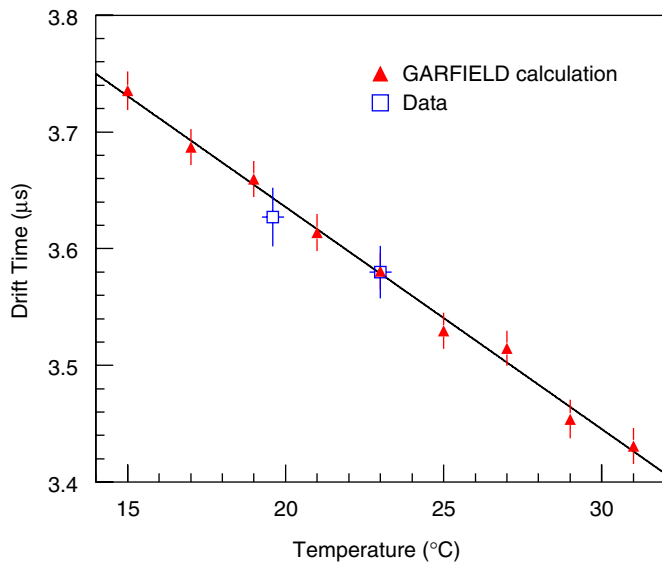
Fig. 10. Drift time variation with DME gas temperature. The plotted drift times are calculated with GARFIELD at a field of 16.4 V/mm for a muon track on the TEC central axis, for various gas temperatures.
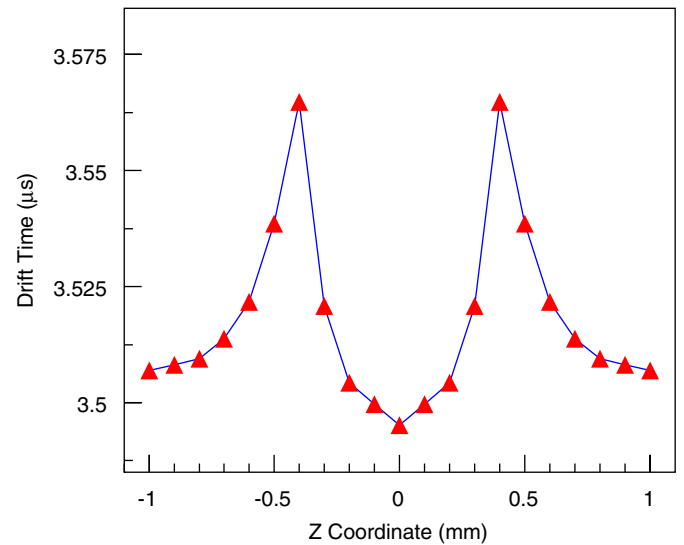

Fig. 11. Dependence of the drift time on z, from a GARFIELD study with drift field 16.4 V/mm for a muon track on the central axis. $z = 0$ mm corresponds to the location of the sense wire and $z = \pm 1$ mm to the adjacent shield wires, while grid wires are at $z = \pm 0.5$ mm (see Fig. 4).

track origin, events with multiple signals in the trigger scintillator, in the event time window, are rejected from the analysis. In the track fitting code, track candidate signals are identified from all wires having signals (hits) within the time window. The drift time is determined with respect to the trigger scintillator time, and then converted to drift distance using the STR. The drift distance, or transverse track position, is then fit versus the z position with a straight line. A straight line is found to be a good approximation even though the solenoid magnetic field extends to the TEC position, where it is typically about 0.1 T and mostly in the z direction.

There are three major contributions to the resolution of the chamber: the spread of drift times in a TEC cell, the multiple scattering effect, and diffusion of electrons. Due to the TEC geometry, drift times within the same cell can vary significantly. Fig. 11, obtained from a GARFIELD study for drift field of 16.4 V/mm, shows the variation of drift time versus z position of ionization. A variation of up to 2% can be seen for an average drift distance, equivalent to 75 ns or about 0.6 mm.

The spatial resolution of an individual TEC cell is determined by fitting the tracks without including hits from that cell and then measuring the residuals. It ranges from 150 to 350 μm, as a function of distance from the sense wire, getting worse with increasing drift distance as shown in Fig. 12. The dependence of hit resolution on drift distance could be caused by transverse and longitudinal diffusion of ionization electrons. The longer the drift, the less likely is the ionization signal to exceed the electronic threshold, due to the fact that diffusion separates the electrons in time.

On average, when there are signals on 18 sense wires in a track, the track angle resolution is ~3 mrad while the
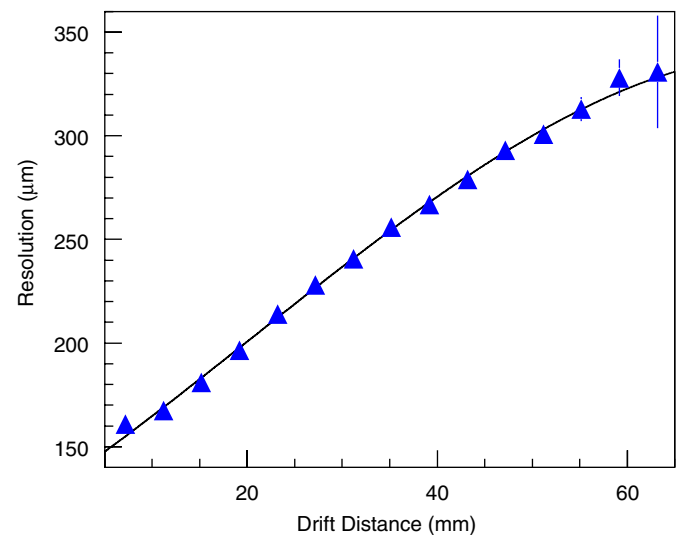

Fig. 12. Measured resolution as a function of track distance from the sense wire.

position resolution, when extrapolated to a plane midway between the two TEC modules, is ~150 μm.

As discussed in Section 2.3, while the tracking efficiency is essentially 100%, the individual sense-wire efficiency is not. Fig. 13 is a measured distribution of the total number of wires with hits (of a maximum possible of 24 wires in a module) for a track as a function of drift distance, where the inefficiency due to the longer drift is clearly visible. Except for this distance correlation, the absence of a hit on a wire seems to occur randomly along the length of the track.
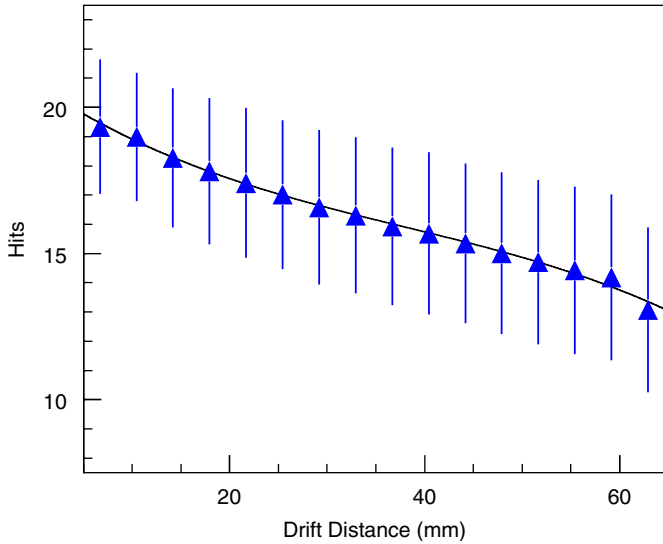
Fig. 13. Total number of valid hits as a function of track distance from the sense wire. Error bars represent rms widths of the hit number distribution.

4. Characterization of the TWIST beam

After alignment and calibration of the TECs, it is possible to obtain and analyze distributions of positions and angles of beam muon tracks, and to measure correlations between them, in a few minutes. A characterization of the muon beam with statistical precision adequate for TWIST simulations can be obtained in a few hours. This section describes typical measurements and how they are used by the TWIST group to adjust the beam and to analyze muon decay data.

4.1. TEC measurements and implications for TWIST

The objectives for beam quality for TWIST were established early in the planning of the experiment. Simulations of a muon beam entering the solenoidal field showed that, to achieve the required small depolarization of order 10^{-3}, the beam should have an rms size of about 5 mm and rms angle of about 15 mrad in the absence of the solenoid field, at a position near the field fringe where radial field components are highest when the solenoid is on. Therefore, the calibration and resolution uncertainties of the TECs must be small compared to these values.

Extensive beam studies based on TEC data without the solenoid field resulted in beam characteristics that satisfied the requirements. The measurement time necessary for a precise measure of means and widths of size and angle distributions, as well as indications of asymmetry or unusual beam shape, was merely minutes. This allowed many different beam tests and adjustments. The effects of slits, apertures, and absorbers in the M13 beam were observed and settings were optimized. Quadrupole steering was minimized, and beam stability over days and weeks was tested. Two surface muon production targets were

used in the studies. The first was an edge-cooled graphite surface muon production target of 10 mm length. The second was a beryllium target of 12 mm length encased in a stainless steel water cooling jacket; it produced an asymmetric x profile some 20% larger than the graphite, thus it is considered inferior for TWIST muon decay measurements.

When the solenoid was turned on to its full 2 T central field, and the STRs from the TEC calibrations were verified to be consistent with those derived with the solenoid off, it was observed that the incoming muon beam was steered to positive values of x and y. Fig. 14 shows an xy beam image with these conditions, from a graphite production target. Note that the intrinsic beam size, without the TEC system, is somewhat smaller than implied by the figure, because some of the multiple scattering produced by the TECs occur prior to tracking in the TEC modules. While the solenoid fringe field does not appreciably alter the beam size, the shift of position away from the solenoid axis, believed to be due to the interaction of the solenoid fringe field with beam quadrupoles and the final beam dipole, is a cause for concern. It reduces the polarization with respect to the solenoid axis (P_μ^z), such that it is less likely to be simulated with the high absolute precision required by TWIST. Steering in the beam line to compensate for the fringe field effect is being implemented for future TWIST measurements.

4.2. Use of TEC data in TWIST simulations

The Monte Carlo simulation of each TWIST event begins with the generation of an input muon. Other beam particles (muons and positrons) are also generated, randomly correlated in time according to measured rates,
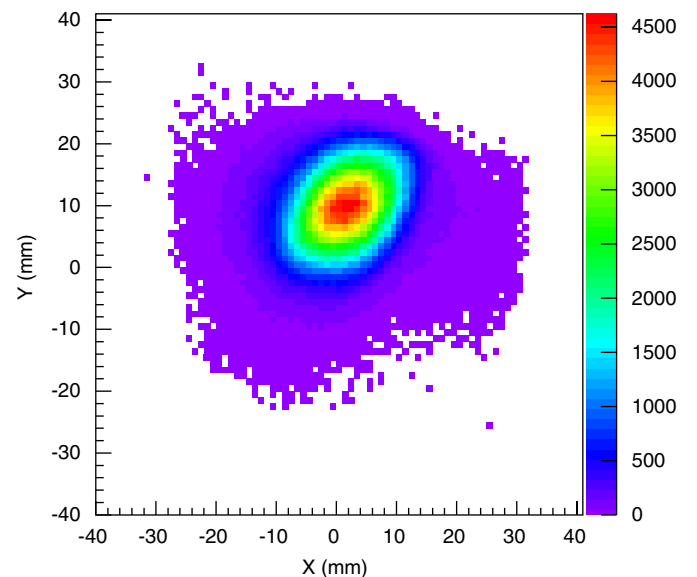

Fig. 14. Two-dimensional distribution of the muon beam intensity at the TEC system, near the fringe field region of the TWIST spectrometer. The pixel size in the figure is $1 \times 1 \, mm^2$.

to simulate the real beam environment. The muon beam distribution in position and angle that is input to this simulation is derived from the TEC measured particle tracks extrapolated to a z position corresponding to a plane between the TEC modules. At this location, multiple scattering has an adequately small effect on the transverse (xy) profile. The angular distributions then contain most of the influence of scattering, and can be modified to account for it to an acceptable level of precision by a quadratic subtraction procedure. This is effectively a deconvolution of the intrinsic beam distribution and the additional broadening of the measured distribution due to scattering, and is carried out in the simulation.

The inputs to the simulation are: the probability of a muon at each xy position as derived from a two-dimensional distribution such as Fig. 14, the mean angles of the muon in x ($\bar{\theta}_x$) and y ($\bar{\theta}_y$) for each xy position as shown in Fig. 15, and the rms of the angle distributions for each xy position. The simulation generates an xy transverse location according to the probability of Fig. 14, using an array with elements of $1 \times 1\,\text{mm}^2$ as shown in the figures. Random Gaussian numbers are generated with mean given by the values of $\bar{\theta}_x$ and $\bar{\theta}_y$ at the xy point as in Fig. 15. The corresponding rms widths used for the random numbers at each xy point are also taken from the TEC information. However, they must be reduced compared to the measured values, to account for the scattering added by the materials of the TECs as the particle passes through; this is accomplished by a quadratic subtraction, using scattering contributions estimated from comparisons of simulations with and without multiple scattering. This technique is intended to reproduce the correlations found between the angles, θ_x and θ_y, and the positions, x and y. Correlations between θ_x and θ_y have been observed to be very small and are not simulated.

The muon is scattered by the TEC gas box entrance window (2.1×10^{-5} radiation lengths) and by 3.5 cm of DME gas (1.3×10^{-5} radiation lengths) before it reaches the TEC X module, resulting in a smearing of the measured θ_x by an estimated 9.5 mrad. Scattering has an even larger influence on the θ_y, smearing it by 12.6 mrad, since the muon travels through an additional 12.0 cm of DME (4.6×10^{-5} radiation lengths) before it reaches the Y module.

Projections of real measured positions and angles are shown in Fig. 16, along with a comparison from a similar analysis of TEC data produced by a simulation that uses the correlated quadratic subtraction of the real distributions as an input. When the distribution of angles for the entire beam is plotted, including this contribution from multiple scattering, the lower two panes of Fig. 16 show a 12.4 mrad rms width for θ_x and a 20.1 mrad rms width for θ_y.

5. Summary

The TEC system has already provided TWIST with important information about the muon beams used to make precise measurements of muon decay as a test of the Standard Model. In the future, we expect to be able to improve the optimization of beam characteristics (beam size and divergence) to provide the smallest possible depolarization of the beam as it enters the solenoidal field of the spectrometer. We will also be able to determine what factors affect the muon beam, and by how much. This in turn will enable us to minimize systematic effects of the muon decay parameter determinations caused by variations in the muon beam, and also to assess accurately the influence of residual systematics. Finally, data from the TECs will be crucial to a reliable simulation of the muon
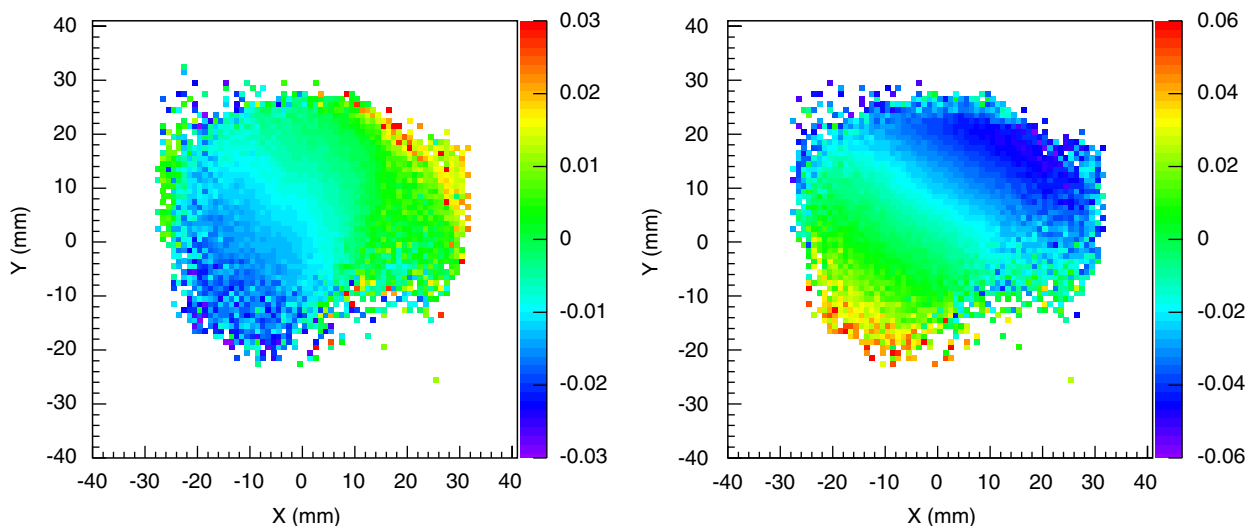

Fig. 15. Two-dimensional distributions of the muon beam mean angle with respect to the z-axis in the xz plane (θ_x, left) and in the yz plane (θ_y, right) for the beam intensity distribution shown in Fig. 14. Note that the color scales, representing the angles in radians, are different to show the trends more clearly. The plots show the rotation of the angle–position correlation due to the fringe field of the solenoid, and the smaller divergence of the beam in the x direction than in y for this particular beam tune.
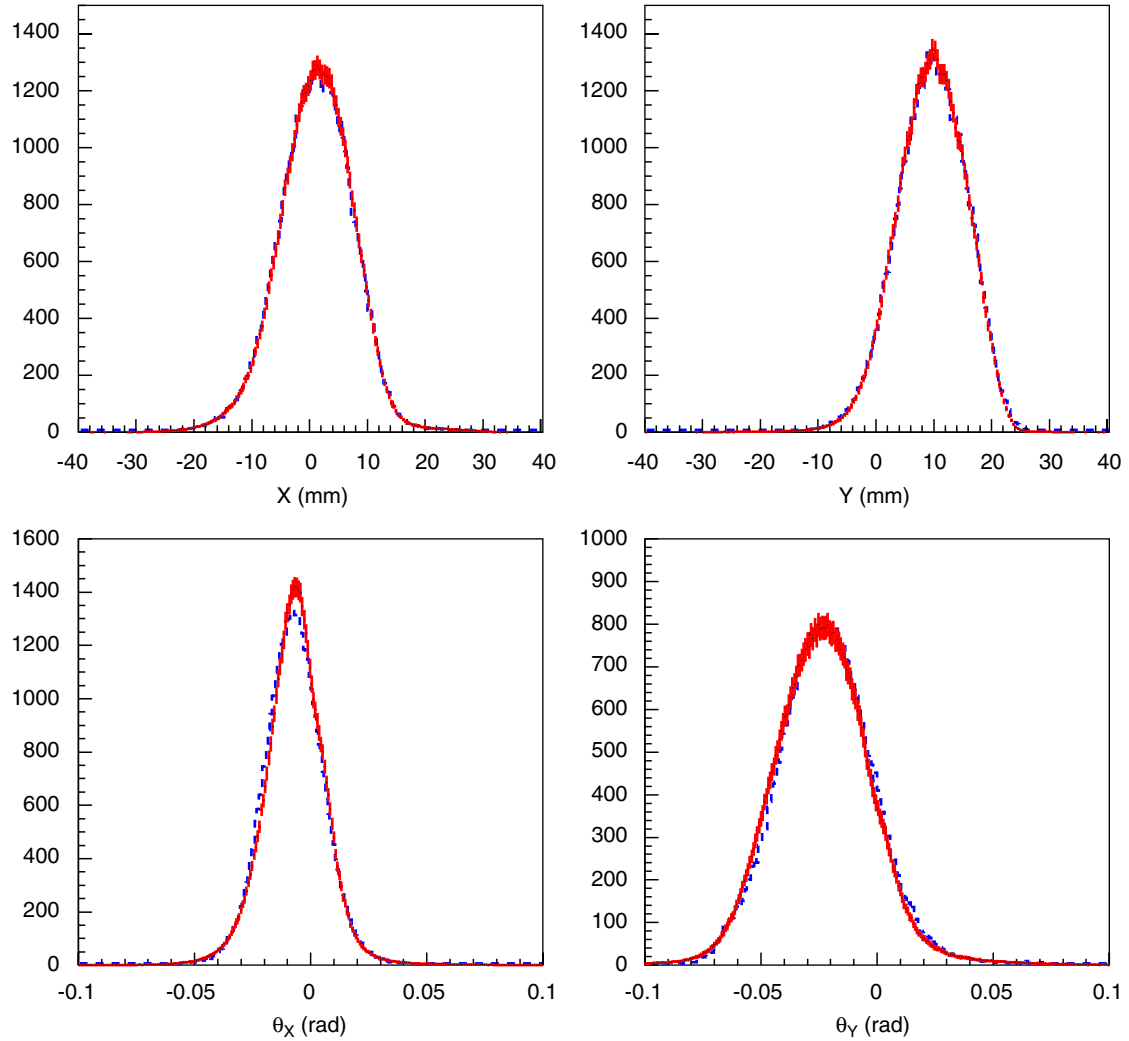
Fig. 16. Distributions in positions and angles of a beam as measured (solid red lines) and as simulated following the quadratic subtraction procedure (dashed blue lines).

beam, which in turn will be necessary for the detailed simulation of all aspects of the experiment. Because the extraction of muon decay parameters from data depends on a high-precision comparison to the simulation, the success of the experiment ultimately will depend in part on the data supplied by the TECs.

Appendix A. Gas flow control

In the TWIST TEC system, flammable DME chamber gas is separated from the cyclotron vacuum by aluminized Mylar windows of $6\,\mu m$ thickness. Consequently, major design features of the gas system include interlocks and procedures to prevent differential pressure from rupturing the $6\,\mu m$ windows and to avoid flammable mixtures of air and DME in the TECs. To provide redundancy, an independent bipolar differential pressure transducer is used to monitor continuously the differential pressure across the windows. A programmable logic controller is used to read the various pressure, flow, and other status inputs and implement the interlock logic. The system has three modes of operation; TEC_Out, Pump/Vent, and Normal Operation.

The TEC_Out mode is used when the TEC gas box has been removed from the vacuum box. Whether or not the TECs are in the vacuum box is detected by a microswitch on the vacuum box mating flange. In this mode, all the

TEC supply and exhaust valves are forced closed, thus isolating the gas system. High voltage to the TECs is disabled. The control system's only active functions are to control in a safe way the gate valve separating the TEC vacuum box from the beam line, and the valve connecting the vacuum box to its vacuum pump and vent ports, with interlocks based on the pressures reported by vacuum gauges in the TEC vacuum box and the beam line.

In the Pump/Vent mode, some valves are forced open, while others are forced closed, such that the TEC gas box and all of the connecting supply and exhaust tubing, which can be at sub-atmospheric pressure during normal operation, can be pumped out through a bypass valve connecting the TEC gas box to the TEC vacuum box. This ensures that possible air leaks into the TECs or any of the connecting plumbing can be discovered. The gate valve is forced closed in this mode, isolating the TEC vacuum box from the beam line during vent and pump down procedures. High voltage to the TECs is disabled. The bypass valve connecting the TEC gas box to the vacuum box can be closed to assist in locating leaks. However, it is forced open if the differential pressure across the windows exceeds a set point limit.

The Normal Operation mode has the most complex interlock scheme. The bypass valve and the valve connecting the vacuum box to the vent and vacuum pump ports cannot be opened. The TEC high voltages are enabled only if all the valves in the gas supply and exhaust lines are open and the DME flow to the TECs exceeds a set point limit (typically $30\,cm^3/min$). The gate valve can be open only if the vacuum box and beam line pressures are satisfactory and the differential pressure across the TEC gas box

windows is below a first set point limit. The gas system valves in the DME supply and exhaust lines can be open only if the vacuum box pressure is satisfactory, and the differential pressure across the windows is below the first set point limit. If despite being isolated from the gas system, the magnitude of the differential pressure continues to increase beyond a second, higher set point limit, the bypass valve connecting the TEC gas box to the vacuum box is forced open to relieve the pressure across the windows. This second limit is set at $\pm 160\,mbar$, well below the $\pm 500\,mbar$ typically required to rupture the windows.

References

[1] L. Michel, Proc. Phys. Soc. A 63 (1950) 514.
[2] C. Bouchiat, L. Michel, Phys. Rev. 106 (1957) 170.
[3] T. Kinoshita, A. Sirlin, Phys. Rev. 108 (1957) 844.
[4] R.L. Henderson, et al., Nucl. Instr. and Meth. A 548 (2005) 306.
[5] TWIST Collaboration, J.R. Musser, et al., Phys. Rev. Lett. 94 (2005) 101805.
[6] TWIST Collaboration, A. Gaponenko, et al., Phys. Rev. D 71 (2005) 071101(R).
[7] TWIST Collaboration, B. Jamieson, et al., submitted, Phys. Rev. D, ⟨http://arxiv.org/abs/hep-ex/0605100⟩.
[8] A. Pifer, T. Bowen, K. Kendall, Nucl. Instr. and Meth. 135 (1976) 39.
[9] C.J. Oram, et al., Nucl. Instr. and Meth. 179 (1981) 95.
[10] A.H. Walenta, IEEE Trans. Nucl. Sci. NS-26.1 (1979) 73.
[11] F. Binon, et al., Nucl. Instr. and Meth. 94 (1971) 27.
[12] A. Breskin, et al., IEEE Trans Nucl. Sci. NS-27 (1980) 133.
[13] R. Openshaw, R. Henderson, Nucl. Instr. and Meth. A 515 (2003) 89.
[14] Y.I. Davydov, et al., Nucl. Instr. and Meth. A 545 (2005) 194.
[15] R.J. Yarema, et al., IEEE Trans. Nucl. Sci. NS-39 (1992) 742.
[16] ⟨http://www.femlab.com/products/multiphysics⟩.
[17] R. Veenhof, GARFIELD, A Drift-Chamber Simulation Program, User's Guide, ver 7.04, CERN, 2001.